J. Electrochem. Sci. Eng. **15(6)** (2025) 2777; http://dx.doi.org/10.5599/jese.2777

Open Access : : ISSN 1847-9286
www.jESE-online.org

Original scientific paper

Carbon paste electrode modified with Bi_2WO_6 nanosheets and ionic liquid: voltammetric assay of dasatinib in the presence of doxorubicin as two anticancer drugs in pharmaceutical and biological samples

Mayada Hadi Al-qassi[1,✉] Wisam Hashim Baqer[2] and Abdul Amir H. Kadhum[3]

[1]*Department of Pharmaceuticals Chemistry College of Pharmacy, Mustansiriyah University, Baghdad Iraq*
[2]*Department of pharmacy, Al-Zahrawi University College: Kerballa, Iraq*
[3]*College of Medicine, University of Al-Ameed, Karbala, Iraq*
Corresponding author: ✉*Mayada.Hadi@uomustansiriyah.edu.iq*

Received: April 10, 2025; Accepted: June 28, 2025; Published: October 3, 2025

Abstract

The main goal of this effort is to create an innovative electrochemical sensor for dasatinib detection in the presence of doxorubicin. It was possible to create Bi_2WO_6 nanosheets easily. The electrochemical performance of the Bi_2WO_6 nanosheets/ionic liquid modified carbon paste electrode (Bi_2WO_6/IL/CPE) was examined in relation to dasatinib detection. Additionally, compared to the unmodified electrode, Bi_2WO_6/IL/CPE demonstrated good electrocatalytic activity for dasatinib oxidation. Under ideal circumstances, the current sensor (Bi_2WO_6/IL/CPE) was investigated using differential pulse voltammetry (DPV). The results showed a linear dynamic range as wide as 0.1-230.0 µM and a limit of detection of 0.05 µM. Additionally, in well-spaced anodic peaks, the Bi2WO6/IL/CPE sensor showed good analytical efficiency for detecting dasatinib in the presence of doxorubicin. This sensor showed two separate peaks for the oxidation of doxorubicin and dasatinib, per the DPV data. Furthermore, the voltammetric measurement of dasatinib and doxorubicin in biological and pharmaceutical specimens was investigated using the Bi_2WO_6/IL/CPE.

Keywords

Electrochemical sensor; chemically modified electrode; real sample analysis; chronoamperometry

Introduction

Due to its aggressiveness and high death rate, ovarian cancer is among the deadliest types of cancer [1]. In the battle against this condition, creating therapeutic drugs and efficient therapies is essential. An oral multitargeted inhibitor of kinases of the SRC family (sarcoma) is dasatinib (DASB) [1]. Tyrosine kinase can be blocked with the use of DASB. It is a traditional anticancer

medication for acute lymphoblastic leukaemia and chronic myelogenous leukaemia [2]. With numerous adverse effects, it is also helpful in the treatment of non-Hodgkin lymphoma, prostate cancer, and metastatic breast cancer. Although patient survival has significantly improved, DASB has been linked to a number of negative side effects, including pulmonary toxicity, gastrointestinal, endocrine, cardiovascular, and hematologic toxicity. Anorexia, dyspepsia, haemorrhagic colonic ulcers, nausea and vomiting, diarrhoea, stomach pain, severe hepatitis, and gastrointestinal bleeding due to platelet failure are a few gastrointestinal adverse effects [2]. Accurately and promptly determining its concentration within the treatment window is crucial due to its toxicity and significant DASB consumption [1,2]. As of right now, spectroscopy [3], chromatography [4], and voltammetry [5] are among the methods used to determine DASB. Nevertheless, there are drawbacks to spectroscopic and chromatographic methods, including costly equipment, sample pretreatments, and laborious procedures. With notable detection limitations, electroanalytical methods are suitable substitutes in this context [5]. In this situation, voltammetric methods are sensitive, selective, and reasonably priced, while electrochemical methods are great choices. Using a range of electrodes, voltammetric techniques have been widely used to evaluate inorganic and organic chemicals and investigate redox reactions due to these advantages [5].

One drug that has shown promise in the treatment of ovarian cancer is doxorubicin (DXN) (Scheme 1) [6]. A common chemotherapeutic medication used to treat cancer of all types, but particularly breast cancer, is DXN [6]. Its chemical composition and mode of action make it an essential component of cancer treatment. By intercalating onto DNA strands and preventing replication, DXN damages DNA in cancer cells [7].

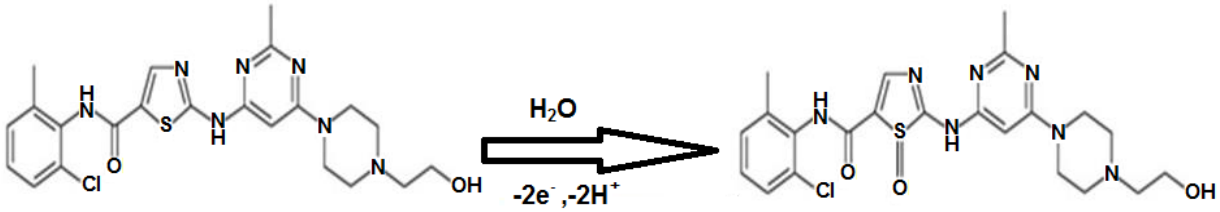

Scheme 1. *Probable electrooxidation mechanism for DASB*

Moreover, it generates reactive oxygen species, which lead to the death of cancerous cells by apoptosis [7]. However, despite its efficacy, DXN has a number of side effects, including cardiotoxicity and myelosuppression [7]. For DXN and related drugs to be administered safely and effectively, precise dosage and level determination are crucial. The significance of establishing the appropriate dosage and monitoring the drug's concentration throughout treatment is emphasized in scientific literature [7]. Many techniques have been reported to be useful for the detection and quantification of DXN and other therapeutics, such as the optical technique, as well as visible spectrophotometry [8], excitation emission matrix fluorescence [9], liquid chromatography combined with tandem mass spectrometry [10], and electrochemical methods [11]. Electrochemical technologies provide the advantages of precision, sensitivity, and ease of usage [11]. There are issues with the DXN detection methods' sensitivity, selectivity, and detection limits. This work presents a new electrochemical sensor which has not been synthesized based on a novel nanocomposite of mesoporous silica and multi-walled carbon nanotubes to overcome these problems [11]. The sensor lowers the detection limit for DXN and considerably expands its analytical linear range, thereby increasing sensitivity and selectivity for DXN detection [11]. One of the acceptable ways to treat ovarian and breast cancer, as the study proved that combining DXN with DASB assists in this treatment, might be inhibiting or reducing proliferation, migration, invasion, as well as cell meta-

bolism by breast cancer cells. Additionally, this combined treatment would help reduce undesirable effects and drug resistance. To guarantee adequate drug levels and therapy optimization, it is crucial to identify such substances in a clinical setting [12].

To create a paste electrode (PE), a solid powder and a pasting liquid are blended to form a heterogeneous mixture, known as a paste mixture [13]. For analytical applications, PEs offer a number of clear benefits, including a broad range of potential windows, low background current, low cost, and an electrode surface that is easily renewable [13]. Many carbon-based materials, including graphite [13], carbon nanotubes [14], graphene [15], and graphene oxide/graphite [16], among others, have been utilized in PE construction to detect pharmaceuticals and biomolecules.

Because of its inherent benefits, which include strong electric conductivity, a broad electrochemical window, low vapor pressure, moderate viscosity, and good chemical and thermal stability, ionic liquids (ILs) have been employed as conductive binders in PEs [17]. Excellent electrochemical performance is demonstrated by IL-carbon PEs, which have a low background current and a quick signal response [17].

Bimetal-based transition metal tungstates have drawn a lot of interest lately [18]. These nanomaterials have a wide range of uses in electronics, sensors, and energy applications because of their unique and promising physicochemical features (environmental friendliness, thermal stability, and chemical stability) [18]. Furthermore, bimetallic nanoparticles (Bi2WO6 NPs) exhibit intriguing photocatalytic, electrocatalytic, and absorption properties and are widely employed in biosensors and biological sensors [19].

To detect codeine in aqueous buffer solutions, the current study aimed to fabricate, design, and evaluate the suitability of a Bi_2WO_6/IL/CPE as a novel electrode. It then evaluated the analytical performance of the Bi_2WO_6 /IL/CPE in quantifying DASB in the presence of DXN. Eventually, the actual samples were analysed to use the newly suggested electrochemical sensor to detect DASB and DXN.

Experimental

Instruments

Autolab 302 N analyser has been used for electrochemical determinations. The three sets of electrochemical cells comprise a Pt wire auxiliary electrode, a carbon paste working electrode, and a saturated calomel reference electrode (SCE).

Synthesis of Bi_2WO_6 nanostructures

With a few minor adjustments, the hydrothermal approach described by Yuan *et al.* [20] was used to create Bi_2WO_6 nanostructures. To create a homogenous solution, 0.12 g of $Na_2WO_4{\times}2H_2O$ and 0.06 g of cetyltrimethylammonium bromide (CTAB) were first mixed in 20 mL of DI water and then agitated for 10 minutes at room temperature. The aforementioned solution was then supplemented with 0.295 g of $Bi(NO_3)_3{\times}5H_2O$. After stirring the liquid for almost an hour, it was sealed in a stainless autoclave lined with Teflon. For ten hours, the autoclave was kept at a temperature of 150 °C. The Bi_2WO_6 nanostructures were obtained by centrifuging the produced sediments after they had cooled to room temperature, washing them five times with ethanol and deionized water, and then vacuum-drying them for 15 hours at 65 °C.

Modified electrode preparation

First, 0.95 g of graphite and 0.05 g of Bi_2WO_6 nanostructures were manually combined in a mortar and pestle. About 0.4 ml of paraffin oil and 0.3 ml of IL were added to the mixture, and it was stirred for 20 minutes to produce a consistently wet paste that was then put into the end of glass tubes. To

maintain the electrical contact, a Cu wire was inserted into the carbon paste. Additionally, more paste was inserted from the tube and polished with a weighing paper to form a fresh surface.

To compare the products, the same method was also used to prepare unaltered CPE without Bi_2WO_6 nanostructures or ionic liquids.

Preparing real specimens

Urine samples from humans were kept in a refrigerator after being collected from the clinical laboratory. 10 ml of the samples were centrifuged for 20 minutes at 2000 rpm. The supernatants were filtered with the use of a filter. The filtered product was diluted five times using phosphate buffer saline (PBS) with a pH 7. The final solutions were then given to the voltametric cell so the analysis could be carried out. At this point, additional treatments are not necessary. The contents of the DASB and DXN samples were determined using the standard addition method.

Following a PBS dilution of 1 ml of doxorubicin injection to 10 ml, different amounts of the diluted solutions were put into a series of 25 ml volumetric flasks and diluted with PBS to the appropriate level.

Five pills of dasatinib, each containing 100 mg, were being ground. Next, 100 mg of the powder was ultrasonically dissolved in 25 ml of deionized water to create the tablet solution. A 25 ml volumetric flask was then filled with varying volumes of the diluted solution, which was then diluted with PBS to the appropriate level.

Results and discussion

Characterization of Bi_2WO_6 nanostructures

XRD analysis was employed to investigate the crystallinity of the as-prepared Bi_2WO_6 nanostructures, and the resulting XRD pattern is presented in Figure 1. The orthorhombic phase of Bi_2WO_6 (JCPDS Card, No. 73-1126) is associated with all the observed diffraction peaks [20-22]. Additionally, the XRD pattern showed no distinctive impurity peaks.

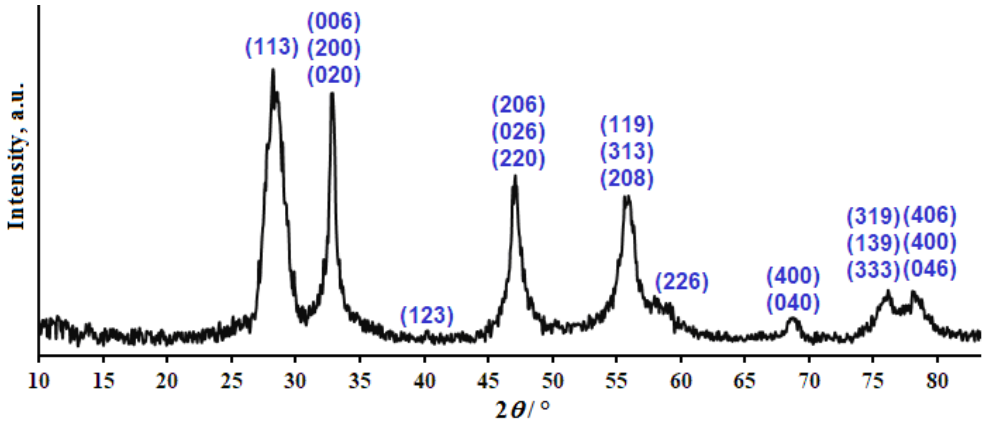

Figure 1. *XRD pattern of Bi_2WO_6 nanostructures*

Electrochemical characteristic of the Bi_2WO_6/IL/CPE

The electrochemical characteristics of Bi_2WO_6/IL/CPE were investigated by cyclic voltammetry (CV) in a 1.0 mM $[Fe(CN)_6]^{3-/4-}$ redox pair (1:1 molar ratio) solution in 0.1 M KCl. To identify the surface area (A), CV was recorded at different scan rates ranging from 5 to 350 mV s^{-1}.

The peak current (I_p) was analysed by the Randles-Ševčik Equation (1) [23]:

$$I_p = \pm(2.690\times10^5)n^{3/2}AD^{1/2}Cv^{1/2} \quad (1)$$

In this equation, D is the diffusion coefficient, which is determined as $D = 7.1\times10^{-6}$ cm^2 s^{-1} and A / cm^2 indicates the area of the electrode. For $K_3[Fe(CN)_6]$, n (number of electrons) equals one. A concen-

tration of $K_3[Fe(CN)_6]$ equal to 0.5 mM is denoted as *C*. The plot slopes of the I_{pa} against $v^{1/2}$ were then used to determine the electroactive regions for Bi_2WO_6/IL/CPE. Additionally, Bi_2WO_6/IL/CPE's electrochemically active surface areas were determined to be 0.29 cm^2. The electroactive surface areas of the bare CPE have been calculated to be 0.1 cm^2.

Electrochemical behaviour of DASB

DASB's electrochemical behaviour (Figure 2) at the unmodified CPE (curve a), Bi_2WO_6/CPE (curve b), IL/CPE (curve c) and Bi_2WO_6/IL/CPE (curve d). The CV was taken at the bare CPE (Figure 2, curve a), and for 100.0 µM DASB in PBS. When compared to the unmodified CPE, the oxidation of DASB at the Bi_2WO_6/IL/CPE surface occurred at a potential of 760 mV, approximately 100 mV more negative. Lastly, DASB's anodic peak currents at Bi_2WO_6/IL/CPE would be 3.35 times higher than those of the bare CPEs. It should be highlighted that the addition of Bi_2WO_6 nanosheets and ILs increased the electrochemical catalytic activities of Bi_2WO_6 /IL/CPE. This is likely due to the increased surface areas that the Bi_2WO_6 nanosheets provide as well as the significant electron transfer capability of the ILs and nanomaterials. Consequently, Bi_2WO_6/IL/CPE significantly increases the electron transfer rates of DASB. The oxidation process at the electrode surface is irreversible since there is no cathodic peak, most probably because the electron transfer is accompanied by a fast follow-up chemical reaction resulting in the inactive product.

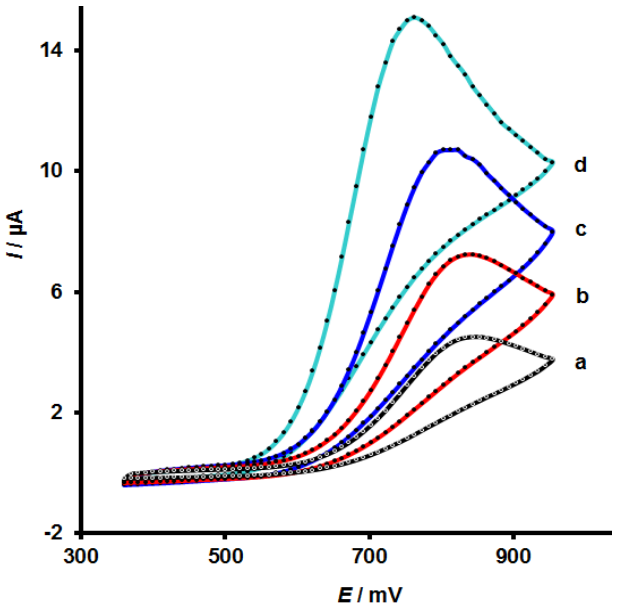

Figure 2. *CVs of unmodified CPE (curve a), Bi_2WO_6/CPE (curve b), IL/CPE (curve c) and Bi_2WO_6/IL/CPE (curve d) in the presence of 100mM DASB in PBS pH 7.0, respectively*

The influence of pH

As demonstrated by comparing the DPV anodic peak potentials of DASB at different pHs in the pH range from 5.0 to 9.0, the electrochemical reaction at the Bi_2WO_6/IL/CPE electrode depends on the pH. Furthermore, the anodic peak potential changed negatively when the solution's pH increased. Figure 3A illustrates the linear relationship between DASB E_{pa} and buffer solution pH. As indicated by the aforementioned -57.679 mV pH^{-1} slope for DASB, the oxidation reaction at Bi_2WO_6/IL/CPE is a pH-dependent reaction that involves equal numbers of protons and electrons. The proposed DASB oxidation mechanism is shown in Scheme 1. At a pH of 7.0, the oxidation's most notable peak current was reached (Figure 3B). Therefore, PBS of pH 7.0 has been used as an electrolyte for further investigations.

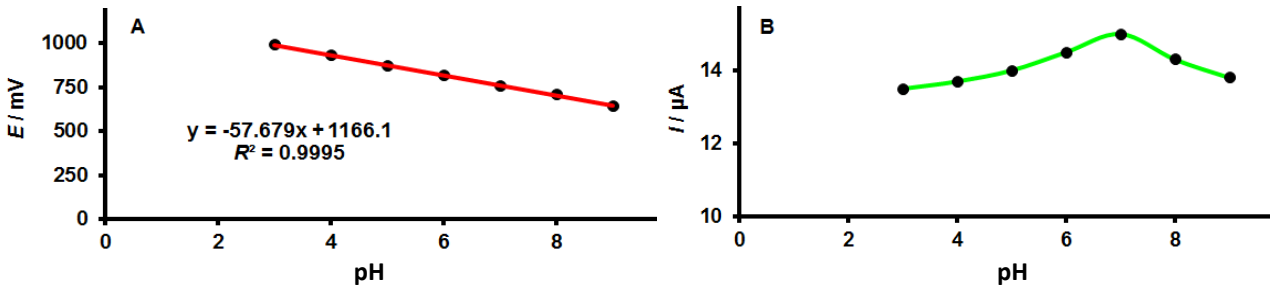

Figure 3. *The electrooxidation diagrams for 100.0 µM DASB in PBS at Bi_2WO_6/IL/CPE show the peak potential-pH (A) and peak current-pH (B) relationships*

The impacts of the potential scan rates

The scan rate that was evaluated on Bi_2WO_6/IL/CPE utilizing linear scan voltammetry (LSV) has an impact on the oxidation peak current of DASB. Figure 4 illustrates the direct proportionality between I_p and v, meaning that a higher peak current intensity was obtained at higher scan rates. Additionally, there is a clear correlation between the I_p and $v^{1/2}$ at the 5 to 400 mV s^{-1} range of scan rates (Figure 4 inset), which indicates a diffusion-controlled reaction. Because Faraday current depends on $v^{1/2}$ and charging current (i_c) is dependent on v, the charging current will noticeably increase at higher scan rates. Based on this, the ideal scan rate for the tests was determined to be 50 mV s^{-1}.

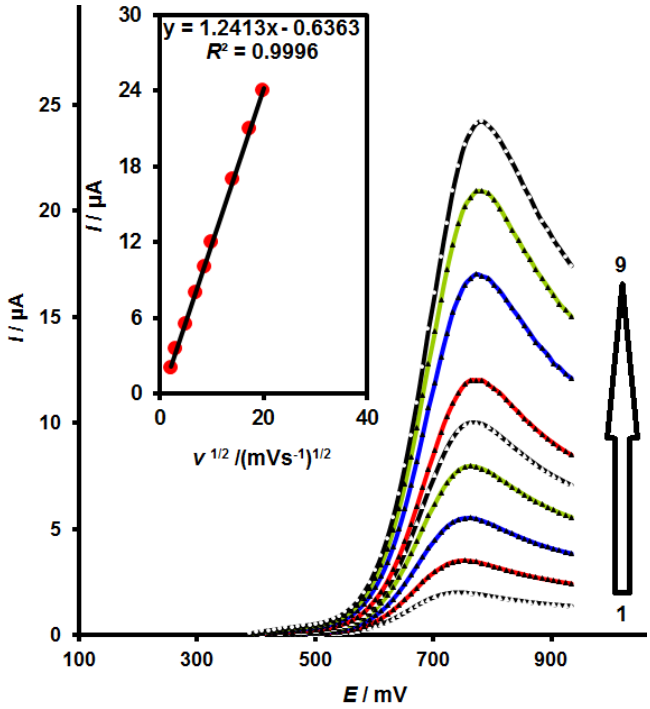

Figure 4. *Linear scan voltammograms of 50.0 µM DASB at Bi_2WO_6/IL/CPE at various scan rates 1 to 9 denotes 5, 10, 25, 50, 75, 100, 200, 300 and 400 mV s^{-1}. Inset: I_{pa} vs. $v^{1/2}$ plot for DASB oxidation at Bi_2WO_6/IL/CPE*

Chronoamperometric studies

By the potential step to 800 mV, the chronoamperometric curves at the Bi_2WO_6/IL/CPE electrodes were recorded at different DASB concentrations (Figure 5).

The *I* for diffusion-controlled electrocatalytic processes of electroactive compounds (*e.g.* DASB) are described by Cottrell's Equation (2) [23]:

$$I = nFAD^{1/2}C_b\pi^{-1/2}t^{-1/2} \quad (2)$$

In Equation (4), the analyte bulk concentrations (mol cm^{-3}) are indicated by C_b, and the number of electrons n = 2. The linear curves from raw chronoamperometric data for various DASB concentrations

were obtained by graphing *I* versus $t^{-1/2}$ (Figure 5A). Next, the DASB concentration was plotted against the slope of the obtained direct lines (Figure 5B). The $D = 2.76\times10^{-6}$ cm^2 s^{-1} was obtained.

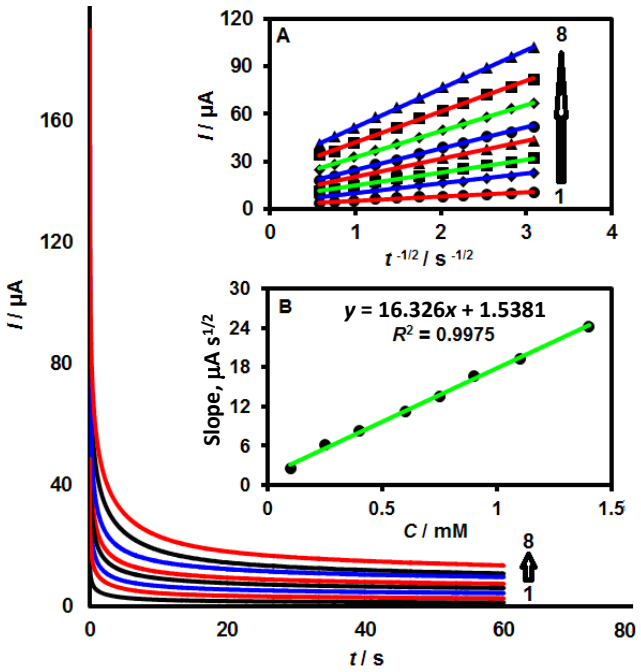

Figure 5. *Chronoamperograms obtained for different DASB concentrations (from inner to outer curve) at the Bi_2WO_6/IL/CPE are 0.1, 0.25, 0.4, 0.6, 0.75, 0.9, 1.1 and 0.14 mM. (A)* I vs. $t^{-1/2}$ *plots derived from chronoamperograms 1 through 8. (B) The straight-line slope plotted versus the concentration of DASB*

Tafel analysis

Transition state theory is a fundamental and generic concept that has been widely applied in the analysis of electrode kinetics. The Tafel equation is given by Equation 3 [23]:

$$\ln i = \ln i_0 + [(1-\alpha)\, nF/RT]\eta \qquad [3]$$

In this equation, α is the transfer coefficient. An exchange current density is represented by i_0. The symbol η denotes overpotential. From the Tafel plot, the transfer coefficient α was calculated to be 0.54 (Figure 6B).

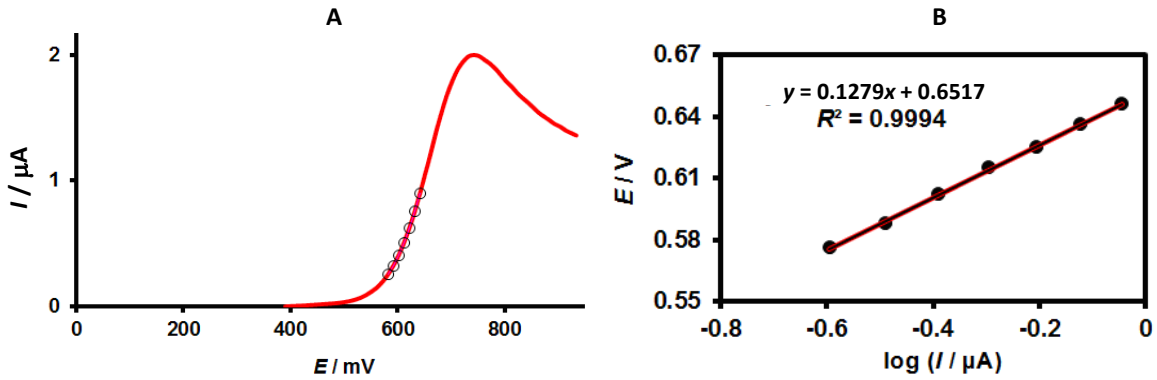

Figure 6. *(A) LSV and (B) Tafel slope of 100.0 µM DASB in PBS pH 7.0 at Bi_2WO_6/IL/CPE*

Determining DASB concentration by voltammetry

Under ideal experimental conditions, DPV was used to determine a DASB calibration plot. Normal DPVs for various DASB concentrations are shown in Figure 7. Ultimately, the linear range from 0.1 to 230.0 µM was produced by the DASB slope value of 0.138 µA µM^{-1}. 0.05 µM has been shown to be the DASB limit of detection (*S*/*N* = 3).

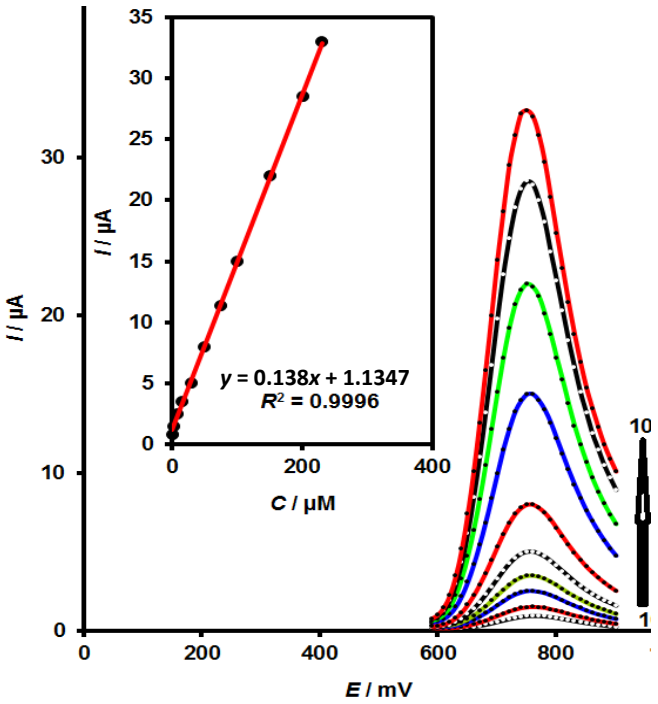

Figure 7. *From number 1 to 10 curve, the DPVs of the Bi_2WO_6/IL/CPE include different concentrations of DASB: 0.1, 2.5, 7.5, 15.0, 30.0, 50.0, 75.0, 100.0, 150.0, 200.0 and 230.0 µM. Inset: Electrocatalytic peak current plotted vs DASB concentration in the 0.1 to 230.0 µM range*

Simultaneous determination of DASB and DXN

As previously mentioned, DASB and DXN coexist in a number of pharmacological environments. As a result, determining DASB and DXN simultaneously was another important aspect for clinical practice. Therefore, using Bi_2WO_6/IL/CPE, the suggested DPV technique was carried out to simultaneously assess DASB and DXN in the synthetic species. Consequently, a concurrent rise in concentrations allowed for the detection of the two analytes (Figure 8).

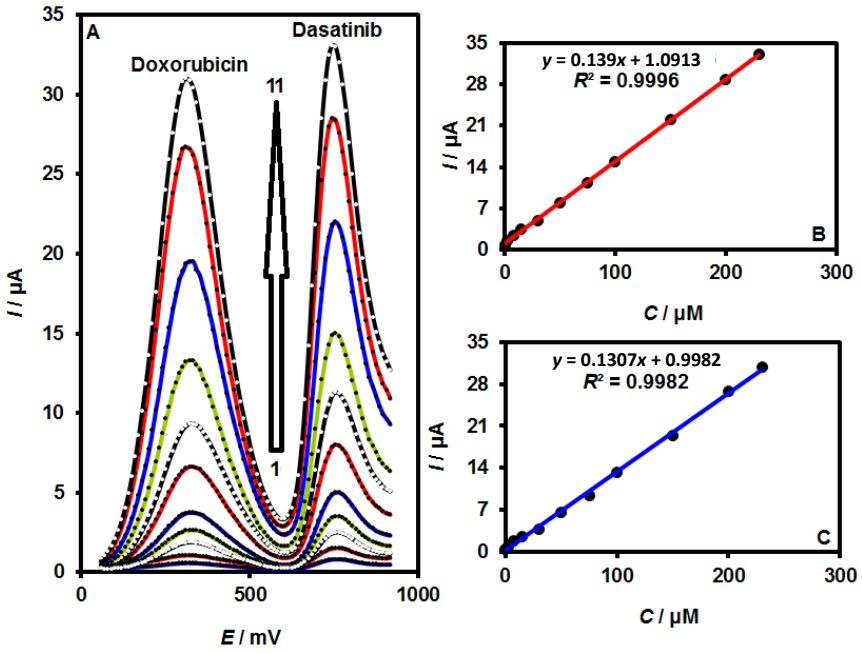

Figure 8. *(A) DPVs of varying DXN and DASB concentrations at Bi_2WO_6/IL/CPE in PBS pH 7.0. Concentrations of DXN and DASB (from inner to outer): (1) 0.1 + 0.1; (2) 2.5 + 2.5; (3) 7.5 + 7.5; (4) 15.0 + 15.0; (5) 30.0 + 30.0; (6) 50.0 + 50.0;(7) 75.0 + 75.0; (8) 100.0 + 100.0; (9) 150.0 + 150.0; (10) 200.0 + 200.0; (11) 230.0 + 230.0 µM. Peak currents vs. concentration of (B) DXN and (C) DASB*

For seven successive detections of 50.0 µM of DASB and DXN, the corresponding standard deviations were 2.0 and 2.3 %, respectively. Therefore, we conclude that DASB and DXN can be determined simultaneously with equal efficiency as when detection is done separately using DPV. The findings showed that the recommended electrode may be effectively used for simultaneous DASB and DXN detection.

Analysing of real samples

To illustrate the usefulness of the method described here, DASB and DXN were found in medication and urine samples at Bi_2WO_6/IL/CPE. Table 1 reports the results of the five parallel detections that were carried out on the samples. Notably, results confirmed that the strategy proposed in the actual specimens was feasible.

Table 1 *Determination of DXN and DASB in real samples using the Bi_2WO_6/IL/CPE (n=5)*

Sample	Amount, µM				Recovery, %		Relative standard deviation, %	
	Spiked		Found					
	DXN	DASB	DXN	DASB	DXN	DASB	DXN	DASB
DXN injection	0	0	2.4	-	-	-	3.0	-
	2.0	5.0	4.5	4.9	102.3	98.0	1.7	3.1
	3.0	6.0	5.2	6.1	96.3	101.7	2.7	2.4
DASB Tablet	0	0	-	4.4	-	-	-	2.6
	5.0	2.0	4.9	6.5	98.0	101.6	2.5	1.9
	7.0	3.0	7.1	7.2	101.4	97.3	2.9	3.3
Urine	0	0	-	-	-	-	-	-
	5.5	6.5	5.7	6.3	103.6	96.9	2.6	1.7
	7.5	8.5	7.4	8.6	98.7	101.2	3.6	2.9

Stability and repeatability of the modified electrodes

Bi_2WO_6/IL/CPE was stored in the room atmosphere. After three weeks, the stability of Bi_2WO_6/IL/CPE was investigated. Cyclic voltammograms showed no change in the oxidation peak potential of DASB. Only the peak currents showed a 2.8 % decrease compared to the initial currents. The CV recording was used to examine the antifouling properties of the modified electrodes regarding the oxidation of DASB and the corresponding oxidation of products. CVs were recorded in the DASB solutions during fifteen cyclic voltammetry cycles. A decrease of less than 2.5 % was noted, even though the alterations were not apparent in the peak potentials. Therefore, using the modified Bi_2WO_6/IL/CPE reduces the corresponding oxidation product fouling effects, improves analyte detection, and enhances sensitivity.

Conclusions

To determine DASB and DXN simultaneously as an electrochemical sensor, a simple one-pot synthesis of Bi_2WO_6 nanosheets was created and put into use, which was unprecedented. In essence, the Bi_2WO_6 nanosheets and ILs have modified carbon paste electrodes that work in tandem to promote mass transport, electrocatalysis, and electron transfer. In terms of sensitivity, the Bi_2WO_6 nanosheets and ILs enhanced the electrochemical reaction of DASB and DXN and significantly reduced the overvoltage. Additionally, DASB and DXN were immediately detected in real specimens using Bi_2WO_6/IL/CPE without the need for treatments, yielding positive findings. This indicates that Bi_2WO_6/IL/CPE is a favourable electrode for the on-site detection of DASB and DXN recreational drugs.

Conflict of interest: *The authors have no conflict of interest.*

References

[1] L. Wang, B. Xiong, W. Lu, Y. Cheng, J. Zhu, G. Ai, Z. Cheng, X. Liu, Z. Cheng, Senolytic drugs dasatinib and quercetin combined with Carboplatin or Olaparib reduced the peritoneal and adipose tissue metastasis of ovarian cancer, *Biomedicine & Pharmacotherapy* **174** (2024) 116474. https://doi.org/10.1016/j.biopha.2024.116474

[2] S. Giebel, M. Labopin, Z. Peric, J. Passweg, D. Blaise, U. Salmenniemi, D. Beauvais, P. Reményi, P. Chevallier, S. Mielke, T, Gedde-Dahl, J. J. Cornelissen, M. Balsat, G. Bug, A. Bazarbachi, E. Brissot, A. Nagler, F. Ciceri, M. Mohty, Impact of the type of tyrosine kinase inhibitor (imatinib or dasatinib) used before allo-HCT on outcome of patients with Philadelphia-positive acute lymphoblastic leukemia. A study on behalf of the Acute Leukemia Working Party of the EBMT, *Transplantation and Cellular Therapy* **31** (2025) 14.e1-14.e10. https://doi.org/10.1016/j.jtct.2024.07.016

[3] T. Kanp, A. Dhuri, M. Aalhate, S. Mahajan, S. Munagalasetty, S. K. Sah, S. Kaity, B. Sharma, V. Bhandari, P. K. Singh, Manifesting the Dasatinib-gallic acid co-amorphous system to augment anticancer potential: Physicochemical characterization, in silico molecular simulation, ex vivo permeability, and in vitro efficacy, *International Journal of Pharmaceutics* **665** (2024) 124672. https://doi.org/10.1016/j.ijpharm.2024.124672

[4] S. Sen, O. P. Ranjan, A Quality by Design (QbD) driven gradient high performance liquid chromatography method development for the simultaneous estimation of dasatinib and nilotinib in lipid nanocarriers, *Journal of Chromatography B* **1243** (2024) 124229. https://doi.org/10.1016/j.jchromb.2024.124229.

[5] C. S. Jesus, V. C. Diculescu, Redox mechanism, spectrophotometrical characterisation and voltammetric determination in serum samples of kinases inhibitor and anticancer drug dasatinib, *Journal of Electroanalytical Chemistry* **752** (2015) 47-53. https://doi.org/10.1016/j.jelechem.2015.06.006

[6] M. Świerczewska, M. Nowacka, P. Stasiak, D. Iżycki, K. Sterzyńska, A. Płóciennik, M. Nowicki, R. Januchowski, Doxorubicin and topotecan resistance in ovarian cancer: Gene expression and microenvironment analysis in 2D and 3D models, *Biomedicine & Pharmacotherapy* **183** (2025) 117804. https://doi.org/10.1016/j.biopha.2024.117804

[7] S. Nandi, N. Kale, A. Patil, S. Banerjee, Y. Patil, J. Khandare, A graphene-sandwiched DNA nano-system: regulation of intercalated doxorubicin for cellular localization, *Nanoscale Advances* **2(12)** (2020) 5746-5759. https://doi.org/10.1039/d0na00575d

[8] C. S. Sastry, J. S. L. Rao, Determination of doxorubicin hydrochloride by visible spectrophotometry, *Talanta* **43** (1996) 1827-1835. https://doi.org/10.1016/0039-9140(96)01932-7.

[9] M. G. Trevisan, R. J. Poppi, Determination of doxorubicin in human plasma by excitation–emission matrix fluorescence and multi-way analysis, *Analytica Chimica Acta*, **493** (2003) 69-81. https://doi.org/10.1016/S0003-2670(03)00864-X

[10] N. Zheng, X. Wang, Y. Wang, G. Xu, H. Zhang, W. Dai, X. B. He, Q. Zhang, J. Ji, Wang, A sensitive liquid chromatography/electrospray tandem mass spectroscopy method for simultaneous quantification of a disulfide bond doxorubicin conjugation prodrug and activated doxorubicin: Application to cellular pharmacokinetic and catabolism studies, *Journal of Chromatography B* **1065** (2017) 96-103. https://doi.org/10.1016/j.jchromb.2017.09.035

[11] N. Erk, G. Kurtay, W. Bouali, A. A. Genç, Molecular binding and electrochemical detection synergy: A study on doxorubicin using nanodiamond-glassy carbon electrodes, *Microchemical Journal* (2025) 112907. https://doi.org/10.1016/j.microc.2025.112907

[12] S. A. Alavi-Tabari, M. A., Khalilzadeh, H. Karimi-Maleh, Simultaneous determination of doxorubicin and dasatinib as two breast anticancer drugs uses an amplified sensor with ionic

liquid and ZnO nanoparticle, *Journal of Electroanalytical Chemistry* **811** (2018) 84-88. https://doi.org/10.1016/j.jelechem.2018.01.034

[13] X. Zhang, S. Duan, X. Xu, S. Xu, C. Zhou, Electrochemical behavior and simultaneous determination of dihydroxybenzene isomers at a functionalized SBA-15 mesoporous silica modified carbon paste electrode, *Electrochimica Acta* **56** (2011) 1981-1987. https://doi.org/10.1016/j.electacta.2010.11.048

[14] R.B. Anagawadi, K. R. Mahanthesha, Glycine functionalized multiwalled carbon nanotube modified carbon paste electrode for the selective determination of Norepinephrine: A Voltammetric study, *Results in Chemistry* **7** (2024) 101479. https://doi.org/10.1016/j.rechem.2024.101479

[15] T. Joseph, N. Thomas, A facile electrochemical sensor based on titanium oxide (TiO_2)/reduced graphene oxide (RGO) nano composite modified carbon paste electrode for sensitive detection of epinephrine (EP) from ternary mixture, *Materials Today: Proceedings* **41** (2021) 606-609. https://doi.org/10.1016/j.matpr.2020.05.257

[16] L. Ding, S. Li, X. Yuan, W. Chang, C. Li, X. Zheng, Preparation and tribological properties of Phenyl-Functionalized thermally reduced GrapheneOxide, *Chemical Engineering Science* **278** (2023) 118869. https://doi.org/10.1016/j.ces.2023.118869

[17] M. Opallo, A. Lesniewski, A review on electrodes modified with ionic liquids, *Journal of Electroanalytical Chemistry* **656** (2011) 2-16. https://doi.org/10.1016/j.jelechem.2011.01.008

[18] Z. Ding, B. Wang, N. Shi, F. Shi, L. Xie, Y. Lai, Y. Wei, L. He, M. Han, W. Huang, Eu-viologen based bimetal–organic frameworks nanosheets with Mn atoms anchored on Eu-μ-O skeletons as high-performance negative electrode for flexible asymmetric supercapacitors, *Chemical Engineering Journal* **497** (2024) 154814. https://doi.org/10.1016/j.cej.2024.154814

[19] R. S. Pedanekar, S. V. Mohite, N. A. Narewadikar, S. B. Madake, Y. Kim, S. J. Kim, S.M. Jokare, K. Y. Rajpure, Photoelectrocatalytic degradation of organic contaminants by spray coated Z-scheme TiO_2/Bi_2WO_6 heterostructure electrode under solar light, *Materials Research Bulletin* **182** (2025) 113127. https://doi.org/10.1016/j.materresbull.2024.113127.

[20] T. Yuan, Z. Li, W. Zhang, Z. Xue, X. Wang, Z. Ma, Y. Fan, J. Xu, Y. Wu, Highly sensitive ethanol gas sensor based on ultrathin nanosheets assembled Bi_2WO_6 with composite phase, *Science Bulletin* **64** (2019) 595-602. https://doi.org/10.1016/j.scib.2019.04.014

[21] J. Wu, F. Duan, Y. Zheng, Y. Xie, Synthesis of Bi_2WO_6 nanoplate-built hierarchical nest-like structures with visible-light-induced photocatalytic activity, *The Journal of Physical Chemistry C* **111** (2007) 12866-12871. https://doi.org/10.1021/jp073877u

[22] R. Tang, H. Su, S. Duan, Y. Sun, L. Li, X. Zhang, S. Zeng, D. Sun, Enhanced visible-light-driven photocatalytic performances using Bi 2 WO 6/MS (M= Cd, Zn) heterostructures: facile synthesis and photocatalytic mechanisms, *RSC Advances* **5** (2015) 41949-41960. https://doi.org/10.1039/C5RA04655F

[23] A. J. Bard, L. R. Faulkner, *Electrochemical Methods: Fundamentals and Applications*, 2nd Edition, J. Wiley & Sons Inc., 2001. ISBN 978-0471043720